Porous activated carbon monolith with nanosheet/ nanofiber structure derived from the green stem of cassava for supercapacitor application

by Rika Taslim

Submission date: 08-Sep-2020 06:31AM (UTC+0700)
Submission ID: 1381605612
File name: Taer_2020_IJER.pdf (2.72M)
Word count: 8890
Character count: 46486

Received: 15 April 2020 | Revised: 9 May 2020 | Accepted: 9 May 2020

DOI: 10.1002/er.5639

RESEARCH ARTICLE

INTERNATIONAL JOURNAL OF ENERGY RESEARCH WILEY

Porous activated carbon monolith with nanosheet/nanofiber structure derived from the green stem of cassava for supercapacitor application

Erman Taer[1] | Novi Yanti[1] | Widya Sinta Mustika[1] | Apriwandi Apriwandi[1] | Rika Taslim[2] | Agustino Agustino[1]

[1]Department of Physics, University of Riau, Riau, Indonesia

[2]Department of Industrial Engineering, State Islamic University of Sultan Syarif Kasim, Riau, Indonesia

Correspondence
Erman Taer, Department of Physics, University of Riau, 28293 Simpang Baru, Riau, Indonesia.
Email: erman_taer@yahoo.com

Summary

Carbonization and activation have been exploited as an economic and efficient approach toward the production of porous activated carbon monolith derived from green stem of cassava (GSC). In addition, $ZnCl_2$ was used as a chemical activator agent at various concentrations, therefore serving as a key factor in the development of porous carbon. The carbonization process (N_2) was integrated with physical activation (CO_2), and then N_2 sorption, scanning electron microscopy, X-ray diffraction, energy dispersive X-ray were examined to evaluate the specific surface area, pore structure characteristic, morphology structure, crystallinity, and the surface element, respectively. Furthermore, cyclic voltammetry was used to measure the electrochemical performance, through a two-electrode system in 1M H_2SO_4. Therefore, the synthesized porous activated carbon exhibits a micropores-mesopores combination, and the optimized sample demonstrated nanosheet and nanofiber structures. The results show a high electrochemical behavior in 1M H_2SO_4 electrolytes, by the electrodes, with specific capacitance, energy, and power densities of 164.58 F g^{-1}, 22.86 Wh kg^{-1}, and 82.38 W kg^{-1}, respectively. This route confirms the opportunity of using novel GSC in the production of porous carbon monolith with nanosheet/nanofiber structure for supercapacitor applications.

KEYWORDS

activated carbon, carbon porous, green stem of cassava, monolith, supercapacitor

1 | INTRODUCTION

Green, renewable, and sustainable sources of energy systems are obtainable through the conversion of wind, water, and solar energy,[1] hence proper capture and storage is required for environmental friendly and economic application.[2] Meanwhile, supercapacitors possessing high power density, high charge-discharge rate, long cycle life, have the ability to store energy in the form of electric charges,[3] by providing a performance between capacitors and batteries. Conversely, the difference between both is that capacitors store and deliver energy incredibly quickly, while batteries have an ability to store high energy densities and also high voltages.[4] However, the main challenge of supercapacitor is related to the energy density entry through the narrow gap of batteries.

Several electrode materials have been developed and suggested to improve energy density, power density, and cycle life of supercapacitor,[5] and three types were identified. These were then classified into carbonaceous

materials or activated carbon,[6,7] conducting polymers,[8,9] as well as transition metal oxides and dichalcogenides (TMDCs).[10,11] Furthermore, the conducting polymers and (TMDCs) were both confirmed to contribute toward specific capacitance, which enable faradaic redox reactions. This results in lower cyclability and changes in cell volume. Based on porosity and adsorptive capabilities, the activated carbon facilitates the formation of double layer for ion storage,[12] leading to the wide development and adoption as a supercapacitor electrode.

Activated carbon typically consists of electrochemical double-layer capacitance (EDLC), ensured by the high porosity, which provide the large specific surface area.[13] This characteristic, alongside the pore size distribution (PSD) play a key role in the improvement of specific capacitance.[14] In addition, the combination of micro and meso or macro pores are known to be beneficial in the production of high energy and power densities required for EDLC. According to International Union of Pure and Applied Chemistry (IUPAC), the pore size of activated carbon is categorized into three types, including micropore (<2 nm), mesopore (2-50 nm), and macropore (>50 nm).[15] Mesopore and macropore are a channel to micropore, which minimize the ion diffusion distances and promote the rate in an electrode material, subsequently increasing the power density.[16]

The development of porosity is obtainable by chemical activation, suggested as a simple and low-cost route, through dehydration and degradation of the precursor structure.[17] This process involves the use of some reagents, including KOH, K_2CO_3, NaOH, H_3PO_4, H_2SO_4, HNO_3, $ZnCl_2$, and others,[18,19] where $ZnCl_2$ possesses the low cost and environmentally friendly characteristics, with the ability to produce a template effect and induce narrow micropores.[7,15,17] In additional, the property also includes the ability to completely volatilize at 756°C, therefore promoting numerous pores.[20] Some studies have reported on the capacity to chemically activate carbon electrode, as seen in orange peels,[7] pine cone,[21] corn straw,[22] seaweed.[23]

Biomass has been identified as the most common precursor, based on the abundance, low cost, simple processing, and usability in a wide temperature range.[24] In addition, activated carbon derived from biomass provides a natural structure and pore, which is disordered by carbon atom and heteroatom,[25] and is known to contain majorly cellulose, hemicellulose, and lignin.[26] In addition, decomposition is attainable by thermal treatment, which is then converted into any functional structure, including nanosheet, nanofiber, and particles.[27,28] These characteristics promote the accessibility of large effective surface, required to improve specific capacitance.[24,29] Meanwhile, some biomass had been reported as successful and effective precursors in the production of activated carbon electrode, derived from agricultural waste,[30] industrial corps,[31] leaves,[32-34] fruit peels,[7,35] fruit shell,[36] flower,[6,37] fruit seeds,[38] stem,[39] wood,[40,41] milk,[42] bagasse.[43,44]

An alternative biomass material is cassava (*Manihot esculenta*), which originates from the tropical countries, including Indonesia.[45] This plant consists of leaves, stem, and the roots, which comprises of food utilization or biopolymer,[38,46] while the peels have been recycled to synthesize supercapacitor electrode and bio-oil.[47,48] In addition, the leaves have been used as a source of nutrient,[49] while its stem has limited applications in advanced product, This part is characterized by two major anatomy, including hard stem, adopted in vegetative reproduction,[45] and the green part, often discarded as useless. Therefore, the development of strategies to utilize the green stem waste in the synthesis of porous activated carbon materials suitable for supercapacitor electrodes is desirable.

This study, therefore, aims at promoting an environmentally and low-cost method, through one stage integrated pyrolysis, in the production of porous activated carbon, using green stem of cassava (GSC) as precursors. The samples were prepared using $ZnCl_2$ for chemical activation at different concentrations (0.1, 0.3, 0.5, and 0.7M), leading to the formation of micropores and mesopores, with average pore diameter in range of 2.28-2.75 nm. The optimized sample of porous activated carbon was found in 0.3M $ZnCl_2$, obtaining a nanosheet/nanofiber structure, which ensures improved specific capacitance. However, the highest specific capacitance of 164.58 F g^{-1} was attained in a two-electrode system, at a scan rate of 1 mV s^{-1}, in the 1M H_2SO_4 electrolyte, showing the most significant energy and power density of 22.86 Wh kg^{-1} and 82.38 W kg^{-1}, respectively. These results indicate the great potential for utilizing GSC in the production of porous activated carbon as an electrode for supercapacitor application.

2 | MATERIALS AND METHODS

2.1 | Electrode preparation

The activated carbon was synthesized from the GSC in several stages, as shown as Figure 1. First, precursors of activated carbon were prepared from GSC biomass (a), which were collected from Riau province, Indonesia. Then, they were cut into a size of ±3 cm, and followed dehydration by sun drying and heating in oven at a temperature of 110°C for 3 days. Second, the material was then precarbonized at a temperature of 250°C for 2.5 hours, and subsequently converted into green carbon

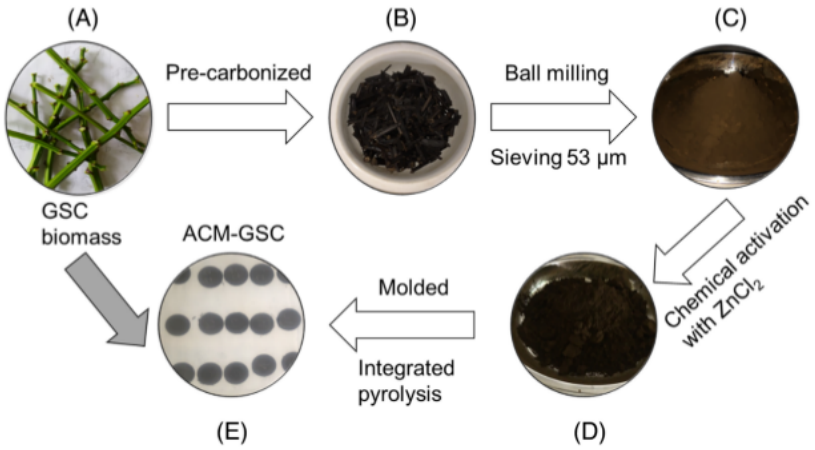

FIGURE 1 Preparation scheme for electrodes [Colour figure can be viewed at wileyonlinelibrary.com]

(b). This was then subjected to ball-milling, followed by sieving, in order to obtain carbon powder of size <53 μm (c). Third, the samples were then chemically activated using $ZnCl_2$ agents (d), and the product was molded into pellets form through a hydraulic press with diameter of ±2 cm. This output was then converted through an integrated pyrolysis method to obtain the activated carbon monolith (ACM) of GSC (e). Finally, the ACM-GSC samples were purified using distilled water to attain a neutral pH, and further polished to achieve a thickness electrode at different concentrations of $ZnCl_2$, that is, 0.1, 0.3, 0.5, and 0.7M. The resulting samples were labeled GSC-X, where X refers to the concentration of activating agent, and all stages were repeated for each sample.

All GSC-X were treated with integrated pyrolysis, which involved both carbonization and physical activation, as illustrated as in Figure 2. In addition, the carbonization process was conducted in two stages, with the characteristic exposure to N_2 gas atmosphere, these include: (1) at soaking temperature, which was initiated at room temperature, up to 288.6°C, leading to the decomposition of carbon compound, producing higher carbon content. (2) Carbonization at a maximum temperature of 600°C, which facilitated the generation of new pores through chemical activation, using $ZnCl_2$. These stages were then followed by physical activation in CO_2 gas atmosphere at 900°C for 2 hours 30 minutes, which caused the enlargement of existing pores. Furthermore, the final stage involved a natural cooling process to room temperatures.

2.2 | Thermal analysis

Thermal analysis was conducted on the GCS samples, using thermogravimetric analysis (TGA) (Shimadzu

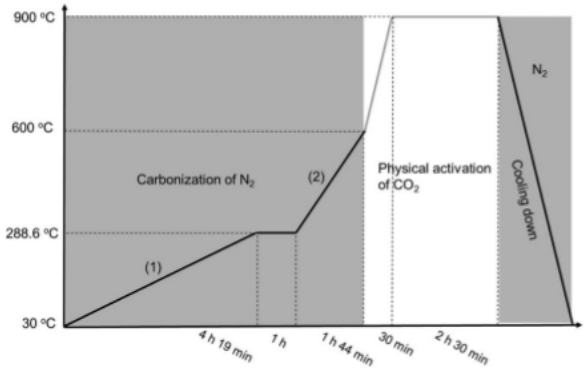

FIGURE 2 Carbonization and physical activation profile

TGA-50), at a heating rate of 10°C/min in nitrogen atmosphere, with flow rate of 100 mL/min. Therefore, analysis for temperature range of 30°C-600°C was performed, using platina as a reference.

2.3 | Structure characteristic

Pellet density was evaluated prior to the carbonation-activation process, using the measure obtained for mass, thickness and diameter, where 20 samples were tested for each GSC-X and the density shrinkage was determined. The textural characteristic, including specific surface area (S_{BET}), total pore volume (V_{TOTAL}), average pore size (D_{AVERAG}) and PSD were measured based on N_2 gas sorption, at a temperature of 77.35 K, using the Quantachrome Instrument TouchWin Version 1.2. Therefore, the Brunauer-Emmett-Teller (BET) equation was used in the calculation of S_{BET} for each sample, while the V_{TOTAL} volumes were estimated from the amount of nitrogen adsorbed at a relative pressure of ~0.95. In addition, the mesopore volume and PSD were calculated using the

Barrett-Joyner-Halanda (BJH) method, and prior to the measurement of N_2 sorption isotherm, all samples were outgassed in the vacuum degassing, in attempts to remove water and other impurities.

The samples were characterized to determine the crystalline degree of the carbon electrodes using the X-ray diffraction (XRD) measurement, carried out with Phillip X-Pert Pro PW3060/10. This assessment was conducted using a source of Cu-Kα radiation (Kα = 1.5418 Å) in the 2θ scale range of 10°-100°, while the interlayer d spacing (d_{002} and d_{100}) was calculated using Bragg's law, determined as follows:

$$n\lambda = 2d\sin\theta, \tag{1}$$

where, n is the mean diffraction order in value, with a maximum order of 1λ, λ denotes the X-ray wavelength for Cu-Kα radiation of 1.5418 Å, while d was defined as the interlayer d spacing, where d_{002} and d_{100} signifies Θ_{002} and Θ_{100}, respectively. Furthermore, θ represents the angle of reflection plane, which is 002 and 100 planes, respectively.

The activated carbon derived from biomass based on amorphous structure is approximated as turbostratic crystallites, for further analysis. This material possessed average crystalline thickness (L_c) and graphene sheet diameter is obtainable, through the empirical expression of Debey-Scherer, following equation.[39,50]

$$L_c = \frac{0.89\lambda}{\beta\cos\theta_{002}}, \tag{2}$$

$$L_a = \frac{1.94\lambda}{\beta\cos\theta_{100}}, \tag{3}$$

L_c and L_a is the mean crystallite dimension in Å along a line normal to the reflecting plane 002 and 100, respectively. β is the full width at half-maximum of the plane in 2θ, while θ denotes the scattering angles (°).

The number of graphitic layers (N) was estimated using the following equation:

$$N = \frac{L_c}{d_{002}}. \tag{4}$$

The morphology of samples was observed via scanning electron microscopy (SEM) (JEOL-JSM-6510LA), embedded with energy dispersive X-ray (EDX) for the analysis of chemical composition. Therefore, the samples were prepared for SEM in monolith form without coating, and the images were obtained with an accelerating voltage of 15 kV, using the secondary electron image.

2.4 | Electrochemical performance

The electrochemical properties were investigated with the cyclic voltammetry (CV) method, using the physics tool CV UR Rad-Er 5841, and controlled with graphical user interface (Cyclic Voltammetry CVv6). This instrument was calibrated to VersaStat II Princeton Applied Research, with an error of ±6.05%, and the measurement was conducted in 1M H_2SO_4 electrolyte, with the voltage range of 0.0 to 1.0 V. Furthermore, this process was also performed in a two-electrode system, assembled with sandwich layer, and immersed in 1M H_2SO_4 electrolyte for 2 days. Conversely, the two thickness GSC electrodes were placed in a two piece current collector (stainless steel), devoid of binders, and separated by egg duck shell separator, prepared using the details of previous work.[51] Therefore, the electrodes, current collector and separators were packaged for supercapacitor cells, using body cell (teflon and acrylic), and the electrochemical performance was then investigated by calculating the specific capacitance, using following the Equation (5).

$$C_{sp} = \frac{I_c - I_d}{m\,x\,s}. \tag{5}$$

The energy and power densities were estimated from CV, using Equations (6) and (7), respectively.

$$E = \frac{1}{2}\,C_{sp}\,\Delta V^2\,x\,\frac{1000}{3600}, \tag{6}$$

$$P = \frac{E}{\Delta t/3600}, \tag{7}$$

where C_{sp} denotes specific capacitance (F g^{-1}), I_c and I_d represent the charge and discharge current (A), respectively, m is the average mass loading of two electrodes (g), and E designates the average energy density of the electrode (Wh kg^{-1}). In addition, ΔV and Δt are the potential window of CV (V), and time for the discharge process (s), respectively, with P representing the average power density (W kg^{-1}).

3 | RESULTS AND DISCUSSION

3.1 | Thermal analysis

The biomass materials contained hemicellulose, cellulose, and lignin, with the capacity of being decomposed into fixed carbon content.[52] In addition, the activated carbon GSC was synthesized following a combination routine route, which includes chemical activation,

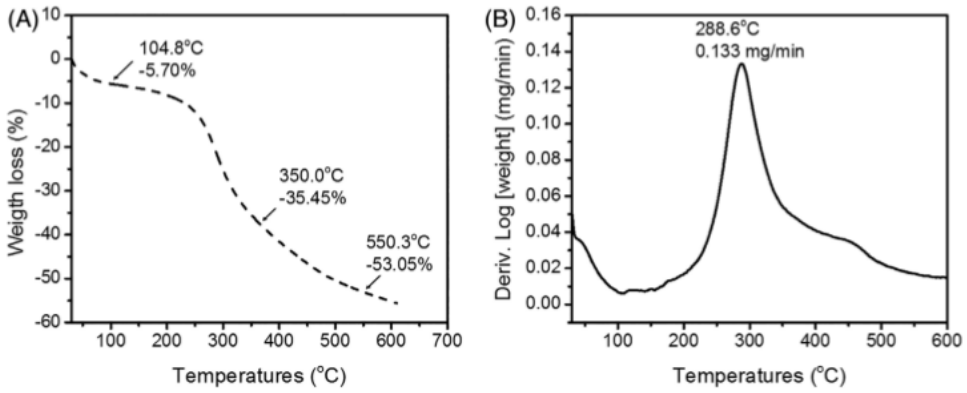

FIGURE 3 Supramolecular changes characterized by; A, thermal gravimetric analysis; B, derivative thermal analysis

carbonization, and physical activation. These stages featured changes in the supramolecular properties investigated, and TGA, as shown in Figure 3A, demonstrates the first raw material decomposition at temperatures reaching 104.8°C. This phase indicated the release of water content, as GSC materials mainly decompose at a range of 200°C-350°C, with a 35.45% weight loss. Ultimately, the hemicellulose component notably degrades at a temperature range of 165°C-220°C,[31] while 240°C-350°C was reported for cellulose. However, a rise of up to 550°C exhibits weight losses of about 53.05%, possibly attributed to lignin degradation at a range of 280°C-500°C.[26] Figure 3B shows sharp peaks, which were attributed to the degradation of cellulose at about 288.6°C, and the zenith point indicates a fixed temperature for the carbonization of samples, required to achieve high carbon content and low volatiles.

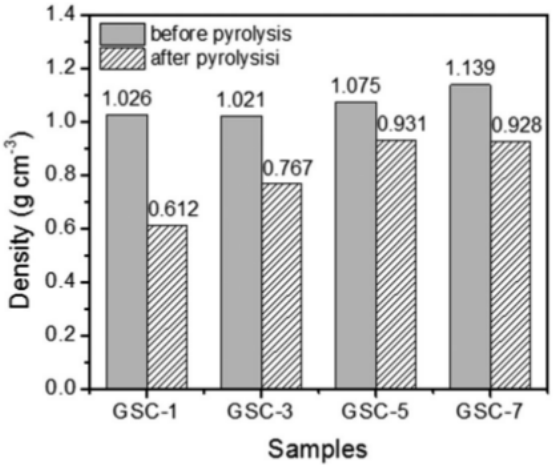

FIGURE 4 Density of GSC monolith by means of before and after pyrolysis. GSC, green stem of cassava

3.2 | Density of monolith

Pyrolysis involving both carbonization and physical activation was a routine adapted to ensure the conversion of biomass to activated carbon. In addition, the purpose of carbonization was to reduce the volatile content and produce char characterized by higher amount of fixed carbon,[53] while the physical activation was proposed for pore development.[17] These processes led to the release of some volatile and a subsequent reduction in the density of GSC pellets, as depicted in Figure 4. Prior to pyrolysis, the density of GSC-1 and GSC-3 were similar, while GSC-5 and GSC-7 were higher, resulting from the increasing concentration of $ZnCl_2$. These changes were attributed to the high molecular weight impregnation of activating agent unto the samples.

Subsequently, the GSC presented with lower density after pyrolysis, resulting from the loss in molecular weight of oxygen, hydrogen, and nitrogen. This phenomenon occurs during carbonization at high temperatures (600°C), which lead to reduced pellet GSC mass, followed by the release of carbon dioxide, through chemical activation of $ZnCl_2$ at 600°C.[13,18] Meanwhile, the physical activation of CO_2 produced carbon monoxide and hydrogen in gaseous phase, which collectively etched the carbon chains, and subsequently generated some vacancies.[17,18] These conditions were attributed to the rearrangement of carbon atom, characterized by the reduction in thickness and diameter of GSC pellets, although the shrinkage in mass was more significant. In addition, the CO_2 gas flow was in the vertically direction to sample surface, featuring a higher reaction with superficial carbon atom than with the horizontal direction.[54]

The changes in density were observed as 40%, 24%, 13%, and 18% shrinkage for GSC-1, GSC-3, GSC-5, and

GSC-7, respectively. Therefore, the $ZnCl_2$ used for chemical activation was transformed into hydrated zinc chloride ($ZnCl_2$.nH2O), and the hydrolysis process generated an interaction between $ZnCl_2$ and oxygen atoms at the sample surface. This leads to the production of oxychloride (ZnOCl), where the Cl element was then released at high physical activation temperatures (above 900°C). Finally, this process causes the formation of carbon atoms and ZnO, which specifically facilitates the generation of new pores.[7,18] Therefore, higher concentrations of $ZnCl_2$ led to a drop in density shrinkage, resulting from the ability to facilitate reactions at the surface of pellets. In addition, it is possible for these impregnation conditions to retain ZnO inside the pellet samples.

Furthermore, the GSC-3 was predicted to achieve well-developed pore structures, which leads to enhanced capacity behavior. The Romero-Rangel model showed the potential for a density of 0.75 g cm^{-3} to result in sponge-like nanoporous carbon structure, affiliated with the manifestation of good interaction with carbon surface. Therefore, higher electronic charge transfer is expected on the amorphous carbon surface,[55] although GSC-5 and GSC-7 demonstrated a relatively higher density of 0.931 and 0.938 g cm^{-3}, respectively, approximated to 1.03 g cm^{-3} from the Romero-Rangel model. These values attribute to low graphitization, and is also associated with larger amorphous ring, reduced ion interaction within the pores, and a decline in capacitance.[55]

3.3 | N_2 absorptions

The N_2 adsorption/desorption isotherms from GSC biomass-derived activated carbon were performed to further analyze the textural properties, including specific surface, as shown in Figure 5A. According to the IUPAC, nitrogen adsorption significant increases in volume at lower relative pressure ($P/P_0 < 0.1$), which is typical for micropores samples. In addition, GSC show a hysteresis loop at high relative pressure ($P/P_0 = 0.4$-0.95), indicating a type IV isotherm for mesopores sorption.[16] The result depicts GSC-1 as type IV isotherm, indicative of mesoporous structure uniformity. Meanwhile, an increase in $ZnCl_2$ concentration for GSC-3 and GSC-7 leads to the illustration of a broad knee of hysteresis at high relative pressure of 0.4 from the GSC isotherms. This indicates the contribution of large micropores, alongside an increase in mesopore development.[56] Hence, GSC samples were observed to have manifested a well-developed combination of micropores and mesopores.

The BJH model was applied to desorption isotherm, for size distribution, as shown in Figure 5B, and the mesopore obtained were 1.78, 1.79, and 1.80 nm, respectively, for GSC-1, GSC-3, and GSC-7. However, the carbonization process conducted at a temperature of 600°C, facilitated the transformation of $ZnCl_2$ to hydrate zinc chloride ($ZnCl_2.nH_2O$), which hydrolyzes and generates oxychloride (ZnOCl), followed by the release of chloride (Cl) and zinc chloride (ZnO) by a thermal process. In addition, the reaction between zinc chloride and carbon atom produces zinc (Zn) and carbon dioxide (CO_2) in the gaseous phase. The reaction etches the carbon atom, leaving numerous vacancies, where ZnO-occupied and Zn-bound are remove by washing, facilitating the generation of micropores on the outer surface of carbon material.[13,18] Furthermore, the physical activation of CO_2 at high temperatures (900°C) is attributed to pore structure development, through (1) the physical activation, which initially opens inaccessible pore, blocked by the disorder of carbon atom and heteroatom. (2) The carbon dioxide (CO_2) reacts with the carbon atom to form gaseous carbon monoxide, and subsequently released via thermal

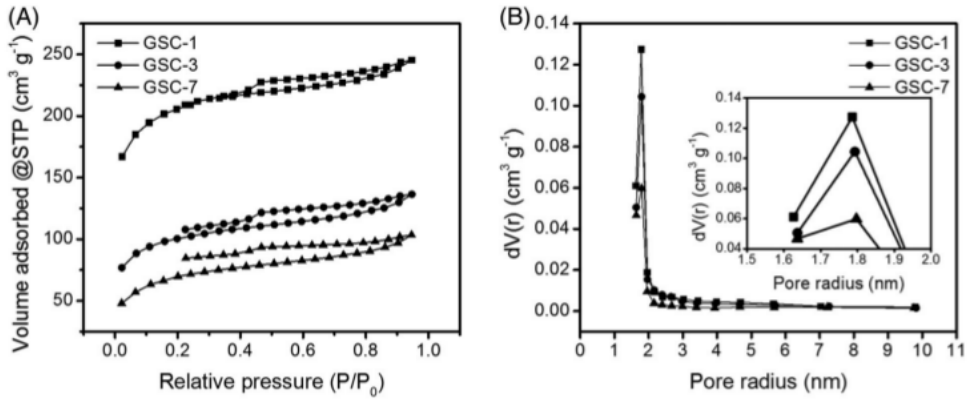

FIGURE 5 A, Nitrogen adsorption-desorption isotherms and B, pore size distribution

TABLE 1 Textural properties of activated carbon monolith derived from GSC

Samples	S_{BET} ($m^2 g^{-1}$)	S_{MICRO} ($m^2 g^{-1}$)	S_{MESO} ($m^2 g^{-1}$)	V_{TOTAL} ($m^3 g^{-1}$)	V_{MICRO} ($m^3 g^{-1}$)	V_{MESO} ($m^3 g^{-1}$)	V_{MICRO}/V_{TOTAL} (%)	V_{MESO}/V_{TOTAL} (%)	D_{AVE} (nm)
GSC-1	666.72	613.72	53.00	0.38	0.32	0.06	84.21	15.79	2.28
GSC-3	329.42	285.44	43.98	0.21	0.16	0.05	76.19	23.81	2.56
GSC-7	233.88	205.77	28.11	0.16	0.13	0.03	81.25	18.75	2.74

Abbreviation: GSC, green stem of cassava.

process. (3) An enlargement of the existed pore is attained by collapsing the walls of adjacent micropores into larger pore.[13,17] Therefore, a combination of chemical activation using $ZnCl_2$ and integrated pyrolysis is expected to produce mesopores carbon materials.

Table 1 shows a summary of the textural properties of GSC samples, as an increase in the concentration of $ZnCl_2$, leads to a decline in the specific surface area (S_{BET}) and total pore volume (V_{TOTAL}). Furthermore, the mesopore surface (S_{MESO}) and mesopore volume (V_{MESO}) also reduced, and micropore formation increased. This condition is expected to increase the number of wall collapse between adjacent pore during physical activation, leading to an enlargement of the larger ones, evidenced by the increase in average pore diameter (D_{AVE}), following the upsurge in $ZnCl_2$ concentrations. For further analysis, the micropore surface (S_{MICRO}) is well defined as a deviation of specific surface area to the mesopore surface (S_{BET} - S_{MESO}),[18] while the micro volume (V_{MICRO}) was calculated as the difference between the total pore volume and mesopore volume (V_{TOTAL} - V_{MESO}).[57] In addition, there was also a decline in the amount and volume of micropore at higher concentrations, which technically provided more significant interactions between the electrolyte ion and carbon surface. These characteristics subsequently generates high energy density, and low ion diffusion. However, the development of mesopores contribute to a reduction in the ion storage pathway, leading to high power density.[15,16,34] Therefore, a combination of micropores and mesopores is expected to produce the best electrochemical performance, as predicted for GSC-3.

3.4 | Scanning electron microscopy

The morphology of GSC samples was observed using SEM, as shown in Figure 6. In addition, the raw materials, activating agent, physical activation were attributed as key factors in morphological modification and also in the development of pore structure in the activated carbon material.[15,25] Meanwhile, the biomass materials constitutes of cellulose, hemicellulose, and lignin, which are possibly converted into fixed carbon content.[29] This occurred due to the structural influence of the pyrolysis route alongside chemical treatment, leading to the formation of nanosheet, nanofiber, nanotubes.[27]

Figure 6A shows the randomly aggregated structure of activated carbon derived from GSC-1, with size ranging from 0.48 to 1.62 μm, featuring some macropores in-between, at 0.30 to 1.08 μm. This configuration was corroborated by the marked region as shown in Figure 6B, with aggregate size and pores ranged from 0.86 to 2.91 μm and 0.73 to 3.36 μm, respectively. In addition, the treatment using pyrolysis and chemical activation with $ZnCl_2$ promoted the opening of inaccessible pores, therefore generating new pores in the GSC-1 sample. The aggregates provide a large specific surface area for the formation of ion pairs, where the macropores are expected to support diffusion into mesopores and micropores.

Furthermore, the increasing concentration of $ZnCl_2$, leads to the formation of larger aggregates in GSC-3, with size ranging from 0.82 to 2.02 μm, and pores spaces of 0.73 to 3.36 μm. Therefore, the increase in chemical treatment using $ZnCl_2$ and physical activation enlarges the existed pore on the carbon surface, which causes erosion and breakage on the outer surface carbon material, due to the corrosive nature of $ZnCl_2$.[58] These conditions are responsible for the transformation of GSC-3 into larger aggregate with larger pores sizes, and a reduction in specific surface area. The marked region in Figure 6D shows a pore size range of 1.23 to 2.56 μm, with increasing concentration of $ZnCl_2$, as newer pores were generated on the outer surface of the GSC carbon materials. These provide accessible active surface area for ion storage, as well as enhanced electrochemical performance.

Moreover, GSC-3 clearly had a unique nanosheet and nanofibers a structure, as seen in the marked region of Figure 6D. This is attributed to the chemical activation of $ZnCl_2$, which possibly extract the supramolecular biomass, subsequently retaining the cellulose and numerous cellulose-lignin linkages. In addition, the solvent extraction was expected to ensure structure modification into nanosheet and nanofiber, and the hemicellulose displayed low molecular weight and short chains, leading to decomposition during the pyrolysis process.[29] These cellulose-based materials, therefore, contribute to the

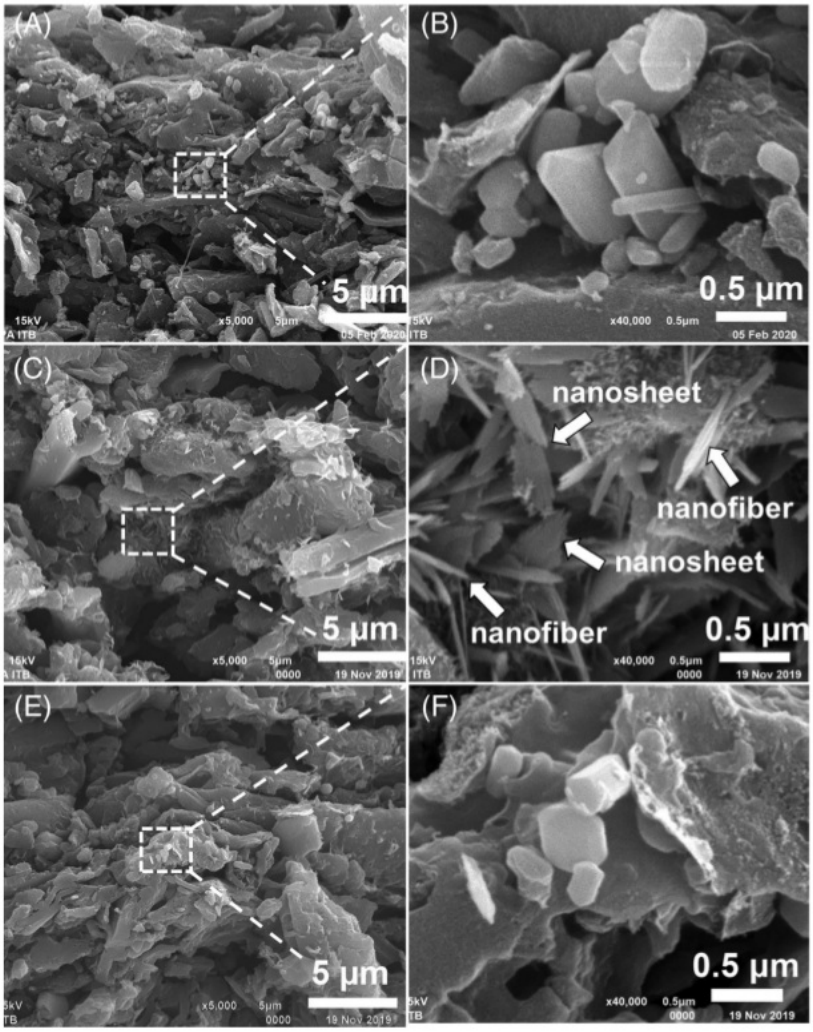

FIGURE 6 SEM images of samples. A, GSC-1; B, enlarged image of the selected region in (A); C, GSC-3; D, enlarged image of the selected region in (C); E, GSC-7; F, enlarged image of the selected region in (E). GSC, green stem of cassava; SEM, scanning electron microscopy

fiber structural form, while lignin was attributed to the nanosheet configuration,[27] whose presence, alongside the nanofiber was related to fast ion diffusion and the high accessible surface for ion pairs.[24,28] Hence, these features, including pores formation onto the aggregate surface and the nanosheet and nanofiber structure, were associated with the generation of high electrochemical performance, as predicted.

At higher concentration of $ZnCl_2$, GSC-7 featured larger aggregates than others, with a size of 1.44-3.91 μm and macropores spaces of 0.62-2.57 μm. This treatment also led to the achievement of larger aggregated-liked structure as seen in the marked region of Figure 6F, demonstrating an aggregate size range of 2.24 to 6.12 μm and pores spaces of 2.47 to 3.50 μm. Furthermore, the gradation in dimension was correlated with the increasing $ZnCl_2$ concentration, as the GSC-7 generated possessed enlarged pores and reduce specific surface area, resulting from the strong corrosive attributes of $ZnCl_2$.[58] In addition, higher concentrations were affiliated with the decomposition of cellulose, which was dependent on the initial composition, hence the nanosheet and nanofiber structure degradation reduced the active surface area for ion diffusion.

3.5 | X-ray diffractogram

The crystalline structures of GSC samples were evaluated using XRD method, as shown in Figure 7, leading to the discovery of two broad peaks around the scattering angles (2θ), and precisely at 25° and 45°. These reflect the carbon planes of 002 (25°) and 100 (45°), which is typical with an amorphous structure of carbon derived biomass. For examples, activated carbon from pine bark was around 2θ to 23° (002) and 44° (100),[59] and the electrode

derived from the biomass of banana stem, corn cob, and potato starch, presented two broad refection peaks around 22°-25° and 43°-45°. These were typically related to highly disordered diffraction planes, corresponding to 002 and 100,[60] and the amorphous carbon is expected to provide high porosity to the carbon electrode, subsequently promoting the generation of large specific surface area.

GSC diffractogram also depicts some sharp peaks indicating carbon sample impurity. Therefore, those observed at 2θ of 28°, and 45° were attributed to a very small amount of silica material in the form of SiO_2 (JCPDS NO.89-1668), while the highest intensity observed at about 2θ of 32° and 48°, was characteristic of zinc oxide (ZnO) (JCPDS-79-2205). Furthermore, others were identified around 36° and 72°, which reflects magnesium oxide (JCPDS card No.89-7746), while those around scattering angles of 37° and 67° indicated calcium oxide (JCPDS No. 82-1690).

Table 2 showed the lattice parameters, including interlayer spacing (d_{002} and d_{100}) and microcrystalline (L_c for stack height and L_a for the stack width) structure, and further analysis was performed on the XRD data in turbostratic crystallite structure. Therefore, the interlayer spacing was calculated from Equation (1), and estimated to around 3.4-3.5 Å (d_{002}) and 2.0 Å (d_{100}), revealing the comparably larger structure of GSC samples than graphite structure (d_{002} = 3.35 Å), which indicate an amorphous structure.[60] For example, activated carbon obtained from the empty fruit bunch of palm oil demonstrated a d_{002} of between 3.692-3.711 Å and d_{100} at 2.0 Å.[54]

As shown in Table 2, the crystallite (L_c) size values of the activated carbons of GSC were small for carbon biomass (L_c = 24.43-37.16 Å), averaging at 6.82-10.11 Å, while 11.35-13.32 Å was reported for the graphene sheet (L_a). For reference purposes, activated carbon derived from the lumpy bracket possess an L_c of 7.58-11.54 Å, while the graphitic layers (N) in the crystallite from ranged from 2 to 3, with the average graphene sheet ranging from 24.43-36.79 Å.[50] The values presented in Table 2 are in line with the conclusions derived from XRD patterns (Figure 7), which attribute the various concentration of $ZnCl_2$ activation with relatively high crystallinity. The activated carbon derived from GSC exhibit the highest average crystallite thickness (L_c), and the average number of graphitic layers (N), alongside low average graphene sheet diameter (L_a). In addition, the low ratio of L_c/L_a predicts elevation in porosity, which was due to the effect of L_c on the specific surface area in the inverse correlation of Kumar empirical formula ($S = 2/(\rho L_c)$), where S is the predicted surface area and ρ is the graphite density.[61]

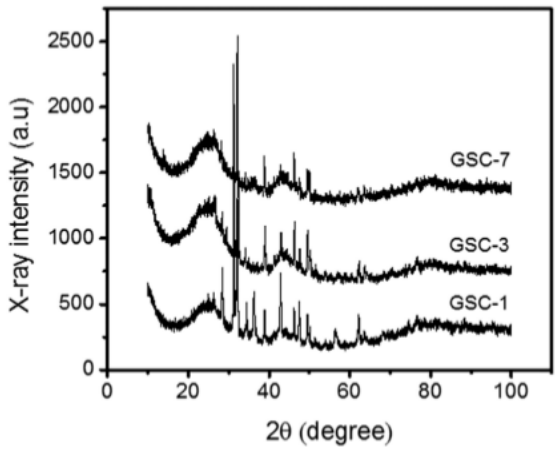

FIGURE 7 XRD curve of activated carbon monolith derived GSC samples. GSC, green stem of cassava; XRD, X-ray diffraction

3.6 | Elemental analysis

The chemical composition of GSC samples were studied from EDX, as shown in Table 3. Therefore, the pyrolysis assisted chemical activation using $ZnCl_2$ led to the production of materials with high carbon content of above 89%, while oxygen was identified as the second dominant element, with a range of 5.12%-7.97%, featuring bad thermal stability at high temperatures.[62] This pyrolysis treatment process possibly causes the release of small amount of oxygen, while chemical activation using $ZnCl_2$ produces ZnO, leading to an exaggerated decline, resulting from the carbon-bond etches and disorders. In addition, there is also a tendency for imperfectly washing to increase the oxygen content. However, lower

TABLE 2 XRD parameters of activated carbon monolith derived from GSC

Samples	$2\Theta_{002}$ (°)	$2\Theta_{100}$ (°)	d_{002} (Å)	d_{100} (Å)	L_c (Å)	L_a (Å)	L_c/L_a	N
GSC-1	25.932	45.872	3.433	1.977	6.828	13.324	0.512	1.989
GSC-3	25.670	45.462	3.468	1.994	8.497	12.102	0.702	2.450
GSC-7	25.232	45.322	3.527	1.999	10.192	11.349	0.898	2.890

Abbreviations: GSC, green stem of cassava; XRD, X-ray diffraction.

concentrations, alongside a decline in surface functional group was attributed to the elevation in electrical conductivity, which subsequently enhances electrochemical capacity.[57]

The activated carbon derived from biomass materials also produces some natural content in low intensity, including some minerals, for example, magnesium, calcium, sodium, potassium, depending on the composition of cultivated soil.[52,63] Furthermore, the limited amount of chlorine and zinc is observed as by-products of ZnOCl, which is not removed by imperfect washing. The values in Table 3 are in line with the conclusions from EDX analysis, which indicate high carbon and oxygen content of GSC samples, alongside the small amount of impurities. Therefore, predictions show the capacity for GSC-3 with the highest and lowest oxygen concentration to promote ion storage, and improve electrochemical performance.

TABLE 3 Chemical composition analysis from EDX

	Atomic weight (%)		
Element content	**GSC-1**	**GSC-3**	**GSC-7**
Carbon	89.80	93.03	90.61
Oxygen	7.97	5.12	6.00
Magnesium	0.49	0.21	0.32
Potassium	–	0.33	0.53
Calcium	0.98	1.21	1.49
Sodium	–	0.10	–
Chlorine	0.42	–	1.05
Zinc	0.33	–	–
Total	100	100	100

Abbreviations: EDX, energy dispersive X-ray; GSC, green stem of cassava.

3.7 | Electrochemical performance

This was evaluated using CV, as the GSC samples were tested in a two-electrode system. The measurements were conducted using the 1M H_2SO_4 electrolyte within the voltage range of 0-1 V, and the CV curves for GSC samples at a constant scan rate of 1 mV s^{-1} was depicted in Figure 8A. These were demonstrated as rectangular-like shapes, which is typically the ideal double-layer capacitance of activated carbon electrode.[34] In addition, the specific capacitance (C_{sp}) (Figure 8A) was calculated using

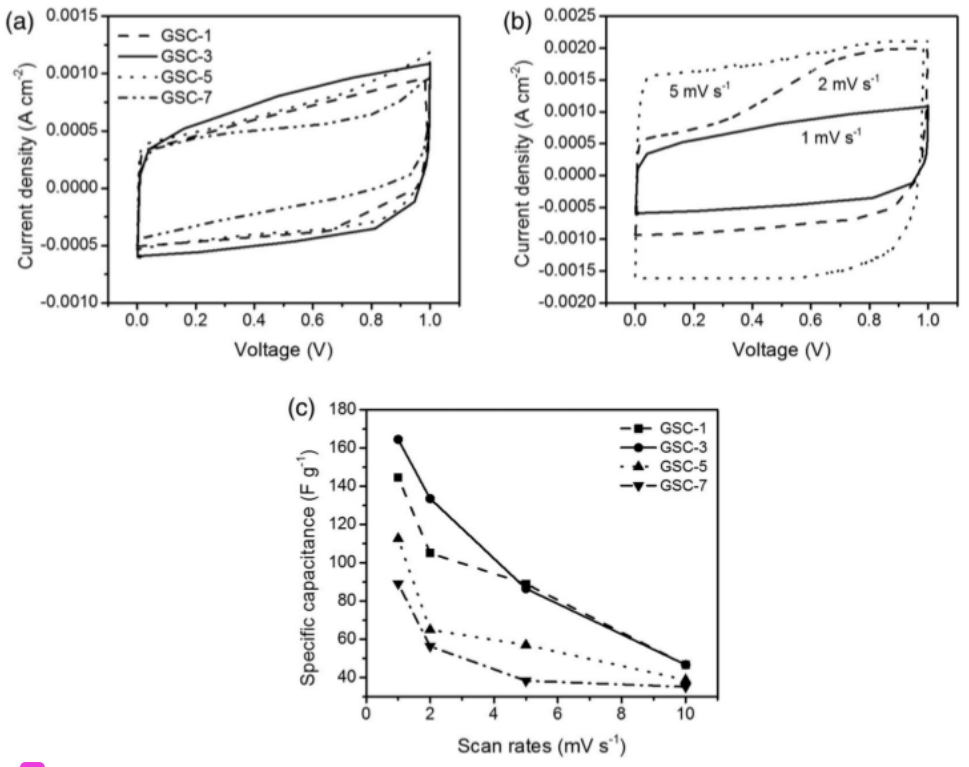

FIGURE 8 Electrochemical measurements in a two-electrode system. A, CV curves of GSC samples at a scan rate of 1 mV s^{-1}. B, CV curve for GSC at different scan rates. C, Specific capacitance at different scan rates. CV, cyclic voltammetry; GSC, green stem of cassava

Equation (5), and the data obtained were 144.65, 164.58, 112.71, and 89.15 F g^{-1}, for GSC-1, GSC-3, GSC-5, and GSC-7, respectively. Hence GSC-3 was concluded to exhibit the highest value, despite the reduction in specific surface area. As previously discussed, the low ratio of micromesopores combination leads to an increase in ion diffusion and storage,[34,64] while the presence of nanosheet and nanofiber structure promote the accessibility to active surface areas.[24,28] Therefore, the specific capacitance was affected by the specific surface area, alongside a well-developed combination of micropores-mesopores and the functional structures of nanosheet-nanofiber, which promotes ion diffusion into the inside pores.[28] Table 4 shows the performance comparison of GSC with the carbon porous reported lastly in the two-electrode system. It performs that GSC exhibits a high specific capacitance of 164.58 F g^{-1}.

As shown in Figure 8B, GSC-3 depicted steady rectangular-like CV curve shapes at different scan rates, ranging from 1 to 5 mV s^{-1}. This condition resulted from the presence of mesopores, which increase the accessibility to active surfaces, subsequently enhancing the ion storage within the micropores. In addition, the macropores plays an important role as transport channels to the mesomicropores, providing rapid ion mobility to the active surface of carbon (see Figure 6). In addition, the nanosheet and nanofiber decorated onto the aggregate surface simply promote accessible interface for fast ion diffusion.

The specific capacitance of GSC samples at different scan rates are shown in Figure 8C, which demonstrate an inverse relationship. Furthermore, a scan rate of 2 mV s^{-1} led to specific capacitance of 72.61%, 81.21%, 57.67%, and 63.20%, for GSC-1, GSC-3, GSC-5, and GSC-7, respectively, while 32.23%, 28.36%, 34.39%, and 39.45% were recorded at the highest value of 10 mV s^{-1}. Therefore, the ion storage capacity was affected by the micropore structure, the presence of mesopores influenced the diffusion rate, due to the reduction in resistivity. Based on previous discussions (see Table 1), it is established that a high microporosity and low mesoporosity of GSC samples reduce the diffusion of ions into the inside micropores.[64]

The samples GSC-1, GSC-3, GSC-5, and GSC-7, respectively, obtained high energy densities of 20.09, 22.86, 15.65, and 12.38 W h kg^{-1}, with power densities of 72.39, 82.38, 56.37, 44.61 W kg^{-1}. These results show that the parameter values are within the range required for the production of activated carbon biomass electrodes, as porous carbon from lignin exhibits an energy and density

TABLE 4 Various biomass-based activated carbon as supercapacitor electrodes

Precursors	Functional structure	Activator agent	S_{BET} (m^2 g^{-1})	V_{TOTAL} (m^3 g^{-1})	D_{AVE} (nm)	Electrolyte	Cs (F g^{-1})	Reference
Tea leaves	–	KOH	911	0.51	<1	6M KOH	167	33
Albizzia flower	microrod	KOH	2757	1.31	2.89	1M Na_2SO_4	58	6
Soybean	–	KOH	1749	–	1.2/3.9	0.5M Na_2SO_4	116	66
Pine sawdust	–	KOH	2331	1.91	3.28	1M KOH	176	41
Lotus leaves	nanoflakes	HNO_3	759	–	–	6M KOH	173	34
Mudstone/lignin	–	HNO_3	4.5	–	–	6M KOH	156	67
Waste tea	–	H_3PO_4	1327	1.14	–	1M H_2SO_4	123	57
Chestnut shell	nanosheet	K_2SO_4	1412	0.75	2.13	6M KOH	216	36
Saccharum bengalense	–	$ZnCl_2$	2090	0.28	2.05	1M Li_2SO_4	103	68
Waste tea	–	$ZnCl_2$	923	0.52	–	6M KOH	140	64
Orange peel	–	$ZnCl_2$	1802	0.88	0.9	6M KOH	221	7
Butnea monosperma pollen		$ZnCl_2$	1422	0.77	2.2	6M KOH	130	69
Pea skin		$ZnCl_2$	1253	0.95	3.04	1M H_2SO_4	193	70
Pine cone	–	$ZnCl_2$	2771	2.12	–	$TEABF_4$	87	21
Rotten carrot		$ZnCl_2$	1155	0.9294	3.22	6M KOH	157	71
Green stem of cassava	–	0.1M $ZnCl_2$	667	0.38	2.28	1M H_2SO_4	144	[This study]
	Nanosheet/nanofiber	0.3M $ZnCl_2$	329	0.21	2.56		164	

of 37.4 and 62 W kg^{-1}.[65] In addition, the records obtained for activated carbon derived from orange peels were 8.3 Wh kg^{-1} and 124.7 W kg^{-1},[7] while the energy density of corn straw was 20.2 Wh kg^{-1}.[22]

4 | CONCLUSION

In summary, porous activated carbon in monolith forms were prepared from the low cost and environmentally friendly precursor of green stem cassava (GSC), through a combination of chemical and physical activation processes. In addition, the agent used was $ZnCl_2$ reagent at different concentrations, and the porous activated carbon derived GSC with 0.3M $ZnCl_2$ (GSC-3) showed the highest specific capacitance, compared with others, despite the possession of a relatively lower specific surface area. Conversely, GSC-3 had a low ratio of micropores (76%) and mesopores (24%), which ensured the adsorption of ions into the inside pores, while the presence of a functional structure (nanosheet and nanofiber) promoted the electrode effectiveness. Furthermore, the optimized electrode displayed high electrochemical behavior in 1M H_2SO_4 electrolytes, with the specific capacitance, energy and power density of 164.58 F g^{-1}, 22.86 Wh kg^{-1}, and of 82.38 W kg^{-1}, respectively. This research provides an economic and efficient route to explore the great potential of novel biomass waste derived from the GSC for possible application in the production of porous activated carbon, as a supercapacitor electrode.

ACKNOWLEDGEMENTS

The authors are grateful to the DRPM Kemenristek-Dikti for the assistance provided in this first year Project of Word Class Research (485/UN.19.5.1.3/PT.01.03/2020), titled “High energy and power densities of supercapacitor for the optimization of the electrode supply process.”

ORCID

Erman Taer https://orcid.org/0000-0003-4463-8252

REFERENCES

1. Wu Y, Zhu J, Huang L. A review of three-dimensional graphene-based materials: synthesis and applications to energy conversion/storage and environment. *Carbon*. 2019;143:610-640.
2. Zakeri B, Syri S. Electrical energy storage systems : a comparative life cycle cost analysis. *Renew Sustain Energy Rev*. 2015;42:569-596.
3. Lefebvre D, Tezel FH. A review of energy storage technologies with a focus on adsorption thermal energy storage processes for heating applications. *Renew Sustain Energy Rev*. 2017;67:116-125.
4. Koohi-Fayegh S, Rosen MA. A review of energy storage types , applications and recent developments. *J Energy Storage*. 2020;27:101047.
5. Khiari B, Jeguirim M, Limousy L, Bennici S. Biomass derived chars for energy applications. *Renew Sustain Energy Rev*. 2019;108:253-2736.
6. Wu F, Gao J, Zhai X, et al. Hierarchical porous carbon microrods derived from albizia flowers for high performance supercapacitors. *Carbon*. 2019;147:242-251.
7. Wei Q, Chena Z, Chenga Y, Wanga X, Yanga X, Wang Z. Preparation and electrochemical performance of orange peel based-activated carbons activated by different activators. *Colloids Surf A*. 2019;574:221-227.
8. Yang L, Henzie J, Park T, et al. Fabrication of flexible microsupercapacitors with binder-free ZIF-8 derived carbon films via electrophoretic deposition. *Bull Chem Soc Japan*. 2020;93:176-181.
9. Wang C, Kim J, Tang J, et al. New strategies for novel MOF-derived carbon materials based on nanoarchitectures. *Chem*. 2020;6:1-22.
10. Septiani NLW, Kaneti YF, Fathoni KB, et al. Self-assembly of nickel phosphate-based nanotubes into two-dimensional crumpled sheet-like architectures for high-performance asymmetric supercapacitors. *Nano Energy*. 2019;67:104270.
11. Makino S, Yamauchi Y, Sugimoto W. Synthesis of electrodeposited ordered mesoporous RuO x using lyotropic liquid crystal and application toward micro-supercapacitors. *J Power Sources*. 2013;227:153-160.
12. Miller EE, Hua Y, Tezel FH. Materials for energy storage: review of electrode materials and methods of increasing capacitance for supercapacitors. *J Energy Storage*. 2018;20:30-40.
13. Li T, Ma R, Lin J, et al. The synthesis and performance analysis of various biomass-based carbon materials for electric double-layer capacitors: a review. *Int J Energy Res*. 2020;44:2426-2454.
14. Iqbal MZ, Zakar S, Haider SS. Role of aqueous electrolytes on the performance of electrochemical energy storage device. *J Electroanal Chem*. 2020;858:113793.
15. Yahya MA, Al-qodah Z, Ngah CWZ. Agricultural bio-waste materials as potential sustainable precursors used for activated carbon production : a review. *Renew Sustain Energy Rev*. 2015;46:218-235.
16. Wei X, Wei J, Li Y, Zou H. Robust hierarchically interconnected porous carbons derived from discarded *Rhus typhina* fruits for ultrahigh capacitive performance supercapacitors. *J Power Sources*. 2019;414:13-23.
17. Gonzalez-Garcia P. Activated carbon from lignocellulosics precursors : a review of the synthesis methods, characterization techniques and applications. *Renew Sustain Energy Rev*. 2018;82:1393-1414.
18. Wang Y, Qu Q, Gao S, et al. Biomass derived carbon as binder-free electrode materials for supercapacitors. *Carbon*. 2019;155:706-726.19.
19. Shanmuga PM, Divya P, Rajalakshmi R. A review status on characterization and electrochemical behaviour of biomass derived carbon materials for energy storage supercapacitors. *Sustain Chem Pharm*. 2020;16:100243.
20. Zhang ZJ, Dong C, Ding XY, Xia YK. A generalized $ZnCl_2$ activation method to produce nitrogen-containing nanoporous carbon materials for supercapacitor applications. *J Alloys Compd*. 2015;636:275-281.

21. Kose KO, Pikins B, Aydinol MK. Chemical and structural optimization of $ZnCl_2$ activated carbons via high temperature CO_2 treatment for EDLC applications. *Int J Hydrogen Energy*. 2018; 43:18607-18616.22.
22. Qiu Z, Wanga Y, Bia X, et al. Biochar-based carbons with hierarchical micro-meso-macro porosity for high rate and long cycle life supercapacitors. *J Power Sources*. 2018;376:82-90.
23. Wang C, Liu T. Nori-based N, O, S, Cl co-doped carbon materials by chemical activation of $ZnCl_2$ for supercapacitor. *J Alloys Compd*. 2017;696:42-50.
24. Selvaraj T, Perumal V, Khor SF, Anthony LS, Gopinath SCB, Mohamed NM. The recent development of polysaccharides biomaterials and their performance for supercapacitor applications. *Mater Res Bull*. 2020;126:110839.25.
25. Zhao X, Chena H, Konga F, et al. Fabrication, characteristics and applications of carbon materials with different morphologies and porous structures produced from wood liquefaction: a review. *Chem Eng J*. 2019;364:226-243.
26. Danish M, Ahmad T. A review on utilization of wood biomass as a sustainable precursor for activated carbon production and application. *Renew Sustain Energy Rev*. 2018;87:1-21.
27. Thomas P, Lai CW, Rafie M, Johan B. Recent developments in biomass-derived carbon as a potential sustainable material for super-capacitor-based energy storage and environmental applications. *J Anal Appl Pyrolysis*. 2019;140:54-85.
28. Mombeshora ET, Nyamori VO. A review on the use of carbon nanostructured materials in electrochemical capacitors. *Int J Energy Res*. 2015;39:1955-1980.
29. Azwar E, Adibah W, Mahari W, Huang J. Transformation of biomass into carbon nanofiber for supercapacitor application: a review. *Int J Hydrogen Energy*. 2018;43:20811-20821.
30. Kumagai S, Tashima D. Electrochemical performance of activated carbons prepared from rice husk in different types of non-aqueous electrolytes. *Biomass Bioenergy*. 2015;83:216-223.
31. Yang X, Kong L, Cao M, Liu X, Li X. Porous nanosheets-based carbon aerogel derived from sustainable rattan for supercapacitors application. *Ind Crops Prod*. 2020;145:112100.
32. Liu Y, Wang Y, Zhang G, Wang D, Dong Y. Preparation of activated carbon from willow leaves and evaluation in electric double-layer capacitors. *Mater Lett*. 2016;176:60-63.
33. Song X, Ma X, Li Y, Ding L, Jiang R. Tea waste derived microporous active carbon with enhanced double-layer supercapacitor behaviors. *Appl Surf Sci*. 2019;487:189-197.
34. Lu Q, Zhou S, Li B, et al. Mesopore-rich carbon flakes derived from lotus leaves and it's ultrahigh performance for supercapacitors. *Electrochim Acta*. 2020;333:135481.
35. Fasakin O, Dangbegnon JK, Momodu DY, et al. Synthesis and characterization of porous carbon derived from activated banana peels with hierarchical porosity for improved electrochemical performance. *Electrochim Acta*. 2018;262:187-196.
36. Hong P, Liu X, Zhang X, et al. Potassium sulphate (K_2SO_4) activation of chestnut shell to oxygen-enriched porous carbons with enhanced capacitive properties. *Int J Energy Res*. 2020; 44(7):5385–5396.
37. Liu Q, Li X, Wu Y, Qing M, Tan G, Xiao D. Pine pollen derived porous carbon with efficient capacitive deionization performance. *Electrochim Acta*. 2019;298:360-371.
38. Kasturi P, Ramasamy H, Meyrick D, Lee YS, Kalai SR. Preparation of starch-based porous carbon electrode and biopolymer electrolyte for all solid-state electric double layer capacitor. *J Colloid Interface Sci*. 2019;554:142-156.
39. Taer E, Taslim R, Mustika WS, Kurniasih B, Agustino AA. Apriwandi Production of an Activated Carbon from a Banana Stem and its Application as Electrode Materials for Supercapacitors. *Int J Electrochem Sci*. 2018;13:8428-8439.
40. Yu F, Ye Z, Chen W, et al. Plane tree bark-derived mesopore-dominant hierarchical carbon for high-voltage supercapacitors. *Appl Surf Sci*. 2019;507:145190.
41. Quan C, Su R, Gao N. Preparation of activated biomass carbon from pine sawdust for supercapacitor and CO_2 capture. *Int J Energy Res*. 2020;44:1-17.
42. Zeng F, Li Z, Li X, et al. Almond-derived origami-like hierarchically porous and N/O co-functionalized carbon sheet for high-performance supercapacitor. *Appl Surf Sci*. 2019;467: 229-235.
43. Guo Y, Tana C, Sun J, Li W, Zhang J, Zhao C. Porous activated carbons derived from waste sugarcane bagasse for CO_2 adsorption. *Chem Eng J*. 2020;381:122736.
44. Tian Q, Wang X, Xu X, et al. A novel porous carbon material made from wild rice stem and its application in supercapacitors. *Mater Chem Phys*. 2018;213:267-276.
45. Ceballos H, Iglesias CA, Perez JC, Dixon AGO. Cassava breeding: opportunities and challenges. *Plant Mol Biol*. 2004;56:503-516.
46. Teixeira EDM, Pasquini D, Curvelo AAS, Corradini E, Belgacem MN, Dufresne A. Cassava bagasse cellulose nanofibrils reinforced thermoplastic cassava starch. *Carbohydr Polym*. 2009;78:422-431.
47. Ismanto AE, Wang S, Soetaredjo FE, Ismadji S. Preparation of capacitor's electrode from cassava peel waste. *Bioresour Technol*. 2010;101:3534-3540.
48. Lu O, Kurniawan A, Xiang C, Ju Y, Ismadji S. Bio-oil from cassava peel: a potential renewable energy source. *Bioresour Technol*. 2013;145:157-161.
49. Santos BRDS, Silva EFR, Minho LAC, et al. Evaluating the chemical profile of the cassava leaves was performed in this work. *Microchem J*. 2020;152:104271.
50. Serafin J, Baca M, Biegun M, Mijowska E, Kale RJ. Direct conversion of biomass to nanoporous activated biocarbons for high CO_2 adsorption and supercapacitor applications. *Appl Surf Sci*. 2019;497:143722.
51. Taer E, Sugianto SMA, Taslim R, Iwantono DD, Deraman M. Eggs Shell membrane as natural separator for supercapacitor applications. *Adv Mater Res*. 2014;896:66-69.
52. Promdee K, Chanvidhwatanakit J, Satitkune S. Characterization of carbon materials and differences from activated carbon particle (ACP) and coal briquettes product (CBP) derived from coconut shell via rotary kiln. *Renew Sustain Energy Rev*. 2017; 75:1175-1186.
53. Qin C, Wang H, Yuan X, Xiong T, Zhang J. Understanding structure-performance correlation of biochar materials in environmental remediation and electrochemical devices. *Chem Eng J*. 2020;382:122977.
54. Farma R, Deraman M, Awitdrus A, et al. Preparation of highly porous binderless activated carbon electrodes from fibres of oil palm empty fruit bunches for application in supercapacitors. *Bioresour Technol*. 2013;132:254-261.
55. Romero-rangel C, Guillén-López A, Mejía-Mendoza LM, Robles M, Espinosa-Torres ND, Muñiz J. Approaches on the

understanding of nanoporous carbon reactivity with polyatomic ions. *Appl Surf Sci*. 2019;495:143392.
56. Yumak T, Yakaboylu GA, Oginni O, Singh K, Ciftyureka E, Sabolsky EM. Comparison of the electrochemical properties of engineered switchgrass biomass-derived activated carbon-based EDLCs. *Colloids Surf A*. 2020;568:124150.
57. Inal IIG, Holmes SM, Banford A, Aktas Z. The performance of supercapacitor electrodes developed from chemically activated carbon produced from waste tea. *Appl Surf Sci*. 2015;357:696-703.
58. Boyjoo Y, Cheng Y, Zhong H, et al. From waste coca cola ® to activated carbons with impressive capabilities for CO_2 adsorption and supercapacitors. *Carbon*. 2017;116:490-499.59.
59. Wang D, Xu L, Nai J, Bai X, Sun T. Morphology-controllable synthesis of nanocarbons and their application in advanced symmetric supercapacitor in ionic liquid electrolyte. *Appl Surf Sci*. 2019;473:1014-1023.
60. Ghosh S, Santhosh R, Jenifer S, et al. Natural biomass derived hard carbon and activated carbons as electrochemical supercapacitor electrodes. *Sci. Rep*. 2019;2019(9):16315.
61. Kumar K, Saxena RK, Kothari R, Suri DK, Kaushik NK, Bohra JN. Correlation between adsorption and x-ray diffraction studies on viscose rayon based activated carbon cloth. *Carbon*. 1997;35:1842-1844.
62. Celiktas MS, Alptekin FM. Conversion of model biomass to carbon-based material with high conductivity by using carbonization. *Energy*. 2019;188:116089.
63. Pallarés J, González-cencerrado A, Arauzo I. Production and characterization of activated carbon from barley straw by physical activation with carbon dioxide and steam. *Biomass Bioenergy*. 2018;115:64-73.
64. Inal IIG, Aktas Z. Enhancing the performance of activated carbon based scalable supercapacitors by heat treatment. *Appl Surf Sci*. 2020;514:145895.
65. Tian J, Liu C, Lin C, Ma M. Constructed nitrogen and sulfur codoped multilevel porous carbon from lignin for high-performance supercapacitors. *J Alloys Compd*. 2019;789:435-442.
66. Lin G, Ma R, Zhou Y, Liu Q, Dong X, Wang J. KOH activation of biomass-derived nitrogen-doped carbons for supercapacitor and electrocatalytic oxygen reduction. *Electrochim Acta*. 2018;261:49-57.
67. Zeng L, Lou X, Zhang J, Wu C, Liu J, Jia C. Carbonaceous mudstone and lignin-derived activated carbon and its application for supercapacitor electrode. *Surf Coat Technol*. 2019;357:580-586.
68. Rawal S, Joshi B, Kumar Y. Synthesis and characterization of activated carbon from the biomass of *Saccharum bengalense* for electrochemical supercapacitors. *J Energy Storage*. 2018;20:418-426.
69. Ahmed S, Ahmed A, Rafat M. Investigation on activated carbon derived from biomass Butnea monosperma and its application as a high performance supercapacitor electrode. *J Energy Storage*. 2019;26:100988.
70. Ahmed S, Ahmed A, Rafat M. Impact of aqueous and organic electrolytes on the supercapacitive performance of activated carbon derived from pea skin. *Surf Coat Technol*. 2018;349:242-250.
71. Ahmed S, Ahmed A, Rafat M. Supercapacitor performance of activated carbon derived from rotten carrot in aqueous, organic and ionic liquid based electrolytes. *J Saudi Chem Soc*. 2018;22:933-1002.

How to cite this article: Taer E, Yanti N, Mustika WS, Apriwandi A, Taslim R, Agustino A. Porous activated carbon monolith with nanosheet/nanofiber structure derived from the green stem of cassava for supercapacitor application. *Int J Energy Res*. 2020;1–14. https://doi.org/10.1002/er.5639

Porous activated carbon monolith with nanosheet/ nanofiber structure derived from the green stem of cassava for supercapacitor application

ORIGINALITY REPORT

15%	7%	13%	%
SIMILARITY INDEX	INTERNET SOURCES	PUBLICATIONS	STUDENT PAPERS

PRIMARY SOURCES

1	Jarosław Serafin, Martyna Baca, Marcin Biegun, Ewa Mijowska et al. "Direct conversion of biomass to nanoporous activated biocarbons for high CO2 adsorption and supercapacitor applications", Applied Surface Science, 2019 Publication	1%
2	Qingjie Lu, Shiqiang Zhou, Bo Li, Haitang Wei, Dongming Zhang, Jicu Hu, Longzhou Zhang, Jin Zhang, Qingju Liu. "Mesopore-rich carbon flakes derived from lotus leaves and it's ultrahigh performance for supercapacitors", Electrochimica Acta, 2020 Publication	1%
3	www.nature.com Internet Source	1%
4	www.journalslibrary.nihr.ac.uk Internet Source	<1%
5	R Taslim, A Agustino, E Taer. "Naturalcarbon-	

	metal composite for supercapacitor application", Journal of Physics: Conference Series, 2018 Publication	<1%
6	R. Farma, M. Deraman, A. Awitdrus, I.A. Talib, E. Taer, N.H. Basri, J.G. Manjunatha, M.M. Ishak, B.N.M. Dollah, S.A. Hashmi. "Preparation of highly porous binderless activated carbon electrodes from fibres of oil palm empty fruit bunches for application in supercapacitors", Bioresource Technology, 2013 Publication	<1%
7	www.hindawi.com Internet Source	<1%
8	Mohd Adib Yahya, Z. Al-Qodah, C.W. Zanariah Ngah. "Agricultural bio-waste materials as potential sustainable precursors used for activated carbon production: A review", Renewable and Sustainable Energy Reviews, 2015 Publication	<1%
9	libtreasures.utdallas.edu Internet Source	<1%
10	Erman Taer, R. Taslim, Sugianto Sugianto, M. Paiszal, Mukhlis Mukhlis, W. S. Mustika, Agustino Agustino. "Meso- and microporous carbon electrode and its effect on the capacitive, energy and power properties of supercapacitor",	<1%

International Journal of Power Electronics and Drive Systems (IJPEDS), 2018
Publication

11	Adekunle Moshood Abioye, Farid Nasir Ani. "Recent development in the production of activated carbon electrodes from agricultural waste biomass for supercapacitors: A review", Renewable and Sustainable Energy Reviews, 2015 Publication	<1%
12	Viengkham Yang, Raja Arumugam Senthil, Junqing Pan, Abrar Khan, Sedahmed Osman, Liren Wang, Wenchao Jiang, Yanzhi Sun. "Highly ordered hierarchical porous carbon derived from biomass waste mangosteen peel as superior cathode material for high performance supercapacitor", Journal of Electroanalytical Chemistry, 2019 Publication	<1%
13	journals.sagepub.com Internet Source	<1%
14	iopscience.iop.org Internet Source	<1%
15	electrochemsci.org Internet Source	<1%
16	elpub.bib.uni-wuppertal.de Internet Source	<1%

17	Xianjun Wei, Ji-Shi Wei, Yongbin Li, Hongli Zou. "Robust hierarchically interconnected porous carbons derived from discarded Rhus typhina fruits for ultrahigh capacitive performance supercapacitors", Journal of Power Sources, 2019 Publication	<1%
18	Zhifei Shan, Shuailong Dai, Yewen Wei, Yuxuan Sun. "Analysis and design of multilayer multiphase interleaved converter for battery pack equalization based on graph theory", International Journal of Energy Research, 2020 Publication	<1%
19	www.drug-dev.com Internet Source	<1%
20	Yuan Gao, Qinyan Yue, Baoyu Gao, Aimin Li. "Insight into activated carbon from different kinds of chemical activating agents: A review", Science of The Total Environment, 2020 Publication	<1%
21	Seiji Kumagai, Masaki Hatomi, Daisuke Tashima. "Electrochemical performance of microporous and mesoporous activated carbons in neat and diluted 1-ethyl-3-methylimidazolium tetrafluoroborate", Journal of Power Sources, 2017 Publication	<1%

22	Xi Yang, Lingyu Kong, Min Cao, Xinge Liu, Xianjun Li. "Porous nanosheets-based carbon aerogel derived from sustainable rattan for supercapacitors application", Industrial Crops and Products, 2020 Publication	<1%
23	Ozge Gorduk, Semih Gorduk, Metin Gencten, Mutlu Sahin, Yucel Sahin. "One-step electrochemical preparation of ternary phthalocyanine/acid-activated multiwalled carbon nanotube/polypyrrole-based electrodes and their supercapacitor applications", International Journal of Energy Research, 2020 Publication	<1%
24	Zhen Zhang, Lei Li, Yan Qing, Xihong Lu, Yiqiang Wu, Ning Yan, Wen Yang. "Manipulation of Nanoplate Structures in Carbonized Cellulose Nanofibril Aerogel for High-Performance Supercapacitor", The Journal of Physical Chemistry C, 2019 Publication	<1%
25	repository.up.ac.za Internet Source	<1%
26	S. Koohi-Fayegh, M.A. Rosen. "A review of energy storage types, applications and recent developments", Journal of Energy Storage, 2020	<1%

Publication

27	Jichao Wang, Xudong zhang, Wen He, Yuanzheng Yue, Yaoyao Wang, Chuanjiang Zhang. " Layered hybrid phase Li NaV (PO) /carbon dot nanocomposite cathodes for Li /Na mixed-ion batteries ", RSC Advances, 2017 Publication	<1%
28	Sonal Singhal, A.K. Shukla. "Improved electrochemical performance of supercapacitors by utilizing ternary Pd-AC-doped NiO nanostructure as an electrode material", Journal of Solid State Electrochemistry, 2020 Publication	<1%
29	www.kacst.edu.sa Internet Source	<1%
30	Yan Ma, Dongling Wu, Tao Wang, Dianzeng Jia. "Nitrogen, Phosphorus Co-doped Carbon Obtained from Amino Acid Based Resin Xerogel as Efficient Electrode for Supercapacitor", ACS Applied Energy Materials, 2019 Publication	<1%
31	escholarship.org Internet Source	<1%
32	www.jmst.org Internet Source	<1%
33	rd.springer.com	

Internet Source

<1%

---

34 Xianyang Meng, Zhiqian Wang, Giuseppe Di Benedetto, James L. Zunino, Somenath Mitra. "Development of nickel-based cable batteries with carbon nanotube and polytetrafluoroethylene enhanced flexible electrodes", International Journal of Energy Research, 2020

Publication

<1%

---

35 www.nims.go.jp

Internet Source

<1%

---

36 Saravanakumar Balasubramaniam, Ankita Mohanty, Suresh Kannan Balasingam, Sang Jae Kim, Ananthakumar Ramadoss. "Comprehensive Insight into the Mechanism, Material Selection and Performance Evaluation of Supercapatteries", Nano-Micro Letters, 2020

Publication

<1%

---

37 Xiao-Li Su, Ming-Yu Cheng, Lin Fu, Jing-He Yang, Xiu-Cheng Zheng, Xin-Xin Guan. "Superior supercapacitive performance of hollow activated carbon nanomesh with hierarchical structure derived from poplar catkins", Journal of Power Sources, 2017

Publication

<1%

Deneb Peredo-Mancilla, Imen Ghouma, Cecile

38	Hort, Camelia Matei Ghimbeu, Mejdi Jeguirim, David Bessieres. "CO2 and CH4 Adsorption Behavior of Biomass-Based Activated Carbons", Energies, 2018 Publication	<1%
39	Cheng Zhu, Tianyu Liu, Fang Qian, T. Yong-Jin Han et al. "Supercapacitors Based on Three-Dimensional Hierarchical Graphene Aerogels with Periodic Macropores", Nano Letters, 2016 Publication	<1%
40	N. L. Panwar, Ashish Pawar. "Influence of activation conditions on the physicochemical properties of activated biochar: a review", Biomass Conversion and Biorefinery, 2020 Publication	<1%
41	www.cheric.org Internet Source	<1%
42	Jiasheng Xu, Yudong Sun, Mingjun Lu, Lin Wang, Jie Zhang, Jianhua Qian, Eui Jung Kim. "Fabrication of porous Mn 2 O 3 microsheet arrays on nickel foam as high–rate electrodes for supercapacitors", Journal of Alloys and Compounds, 2017 Publication	<1%
43	eprints.nottingham.ac.uk Internet Source	<1%

44	Zhenfen Lin, Liyun Ma, Qingwen Wang, Liping Li. "Preparation and characterization of capric-myristic-stearic acid eutectic/mesoporous carbonized pomelo peel as a novel shape-stable composite phase change materials", Materials Research Express, 2019 Publication	<1%
45	Katchala Nanaji, Varadaraju Upadhyayula, Tata Narasinga Rao, Srinivasan Anandan. "Robust, Environmentally Benign Synthesis of Nanoporous Graphene Sheets from Biowaste for Ultrafast Supercapacitor Application", ACS Sustainable Chemistry & Engineering, 2018 Publication	<1%
46	www.frontiersin.org Internet Source	<1%
47	Serdar Altin, Erdinç Öz, Sebahat Altundağ, Ali Bayri et al. "Investigation of hybrid-capacitor properties of ruthenium complexes", International Journal of Energy Research, 2019 Publication	<1%
48	www.scribd.com Internet Source	<1%
49	Arthi Gopalakrishnan, Aimin Yu, Sushmee Badhulika. "Facile synthesis of highly porous N-doped carbon nanosheets with silica	<1%

nanoparticles for ultra-high capacitance supercapacitors", Energy & Fuels, 2020
Publication

50	Yi Lin, Zeyu Chen, Chuying Yu, Wenbin Zhong. "Heteroatom-Doped Sheet-Like and Hierarchical Porous Carbon Based on Natural Biomass Small Molecule Peach Gum for High-Performance Supercapacitors", ACS Sustainable Chemistry & Engineering, 2019 Publication	<1%
51	eeeweba.ntu.edu.sg Internet Source	<1%
52	acris.aalto.fi Internet Source	<1%
53	Kumar, K.. "Correlation between adsorption and x-ray diffraction studies on viscose rayon based activated carbon cloth", Carbon, 1997 Publication	<1%
54	Abioye, Adekunle Moshood, and Farid Nasir Ani. "Recent development in the production of activated carbon electrodes from agricultural waste biomass for supercapacitors: A review", Renewable and Sustainable Energy Reviews, 2015. Publication	<1%
55	Xi Zhang, Hewei Liu, Xuezhen Huang, Hongrui Jiang. "One-step femtosecond laser patterning	<1%

of light-trapping structure on dye-sensitized solar cell photoelectrodes", Journal of Materials Chemistry C, 2015
Publication

---

56 J. P. Tey, M. A. Careem, M. A. Yarmo, A. K. Arof. "Durian shell-based activated carbon electrode for EDLCs", Ionics, 2016 <1%
Publication

---

57 Chun Wu, Shaoran Yang, Junjie Cai, Qiaobao Zhang, Ying Zhu, Kaili Zhang. "Activated Microporous Carbon Derived from Almond Shells for High Energy Density Asymmetric Supercapacitors", ACS Applied Materials & Interfaces, 2016 <1%
Publication

---

58 Xianjun Wei, Hongli Zou, Shuyan Gao. "Chemical crosslinking engineered nitrogen-doped carbon aerogels from polyaniline-boric acid-polyvinyl alcohol gels for high-performance electrochemical capacitors", Carbon, 2017 <1%
Publication

---

59 journalarticle.ukm.my <1%
Internet Source

---

60 Ndeye F. Sylla, Ndeye M. Ndiaye, Balla D. Ngom, Bridget K. Mutuma, Damilola Momodu, Mohamed Chaker, Ncholu Manyala. "Ex-situ nitrogen-doped porous carbons as electrode <1%

materials for high performance supercapacitor", Journal of Colloid and Interface Science, 2020
Publication

61	E Taer, D A Yusra, Apriwandi, Awitdrus, R Taslim, Agustino. "The Effects of Different Activation Agents on the Physical and Electrochemical Properties of Carbon Electrodes Produced from Banana Stem Fiber", Journal of Physics: Conference Series, 2019 Publication	<1%

62	chemistry-europe.onlinelibrary.wiley.com Internet Source	<1%

63	Antonio Rosato, Antonio Ciervo, Giovanni Ciampi, Michelangelo Scorpio, Francesco Guarino, Sergio Sibilio. "Impact of solar field design and back-up technology on dynamic performance of a solar hybrid heating network integrated with a seasonal borehole thermal energy storage serving a small-scale residential district including plug-in electric vehicles", Renewable Energy, 2020 Publication	<1%

64	Handbook of Polymer Nanocomposites Processing Performance and Application, 2015. Publication	<1%

65	Tinesha Selvaraj, Veeradasan Perumal, Shing Fhan Khor, Leonard Sean Anthony, Subash	<1%

C.B. Gopinath, Norani Muti Mohamed. "The recent development of polysaccharides biomaterials and their performance for supercapacitor applications", Materials Research Bulletin, 2020
Publication

---

66 Mao-Cheng Liu, Chun Lu, Yan Xu, Yu-Xia Hu et al. "Three-Dimensional Interconnected Reticular Porous Carbon From Corn Starch By a Sample Sol–Gel Method Toward High-Performance Supercapacitors With Aqueous and Ionic Liquid Electrolytes", ACS Sustainable Chemistry & Engineering, 2019 <1%
Publication

---

67 Zan Gao, Yunya Zhang, Ningning Song, Xiaodong Li. "Biomass-derived renewable carbon materials for electrochemical energy storage", Materials Research Letters, 2016 <1%
Publication

---

68 Dongling Wu, Jinyan Cheng, Tao Wang, Penggao Liu, Liu Yang, Dianzeng Jia. "A Novel Porous N- and S-Self-Doped Carbon Derived from Chinese Rice Wine Lees as High-Performance Electrode Materials in a Supercapacitor", ACS Sustainable Chemistry & Engineering, 2019 <1%
Publication

69	Advanced Structured Materials, 2015. Publication	<1%
70	Ping Cheng, Ting Li, Hang Yu, Lei Zhi, Zonghuai Liu, Zhibin Lei. "Biomass-Derived Carbon Fiber Aerogel as a Binder-Free Electrode for High-Rate Supercapacitors", The Journal of Physical Chemistry C, 2016 Publication	<1%
71	Erman Taer, Rika Taslim. "Brief review: Preparation techniques of biomass based activated carbon monolith electrode for supercapacitor applications", AIP Publishing, 2018 Publication	<1%

Exclude quotes	On	Exclude matches	Off
Exclude bibliography	On		